Mixed Convection of Opposing/Assisting Flows in Vertical Channels with Discrete Asymmetrically Heated Ribs

Tsang-Yuan Lin* and Shou-Shing Hsieh†
National Sun Yat-Sen University, Kaohsiung, Taiwan 80424, Republic of China

Both qualitative flow visualization as well as laser holographic interferometry and quantitative temperature measurement are presented for mixed convection of air layers in vertical channels (channels A and B) with asymmetrical discrete heated ribs, wherein the opposing flow is in channel A and the assisting flow is in channel B. In the case of opposing mixed convection flow, the main flow separates on the heated rib and the recirculatory secondary flow is produced in between two consecutive ribs. However, when the main flow assists buoyancy, the separation takes place on the cold wall and a secondary flow exists in a region away from the heated rib. Based on the analyses of the photographs and interferograms, it is found that, as Gr/Re^2 increases, the recirculation becomes stronger and the region becomes smaller for assisting flow (in channel B), whereas this change seems unclear for the opposing flow (in channel A). However, the heat transfer rates in channel A are consistently higher than those in channel B for the cases under investigation. The result might be useful for the thermal design configuration of coolings of electronic equipment.

Nomenclature

A_h = surface area of the rib, m²
C = isobaric specific heat, J/kg.K
D = depth of channel in z direction, m
D_h = hydraulic diameter, m
Gr = Grashof number, $= g\beta (T_w - T_o)D_h^3/\nu^2$
g = acceleration due to gravity, m/s²
H = height of the channel, m
h = local heat transfer coefficient, $= Q_c/A_h(T_w - T_o)$
k = thermal conductivity, W/m.K
L = length of the channel, $= 2H$, m
L_1 = length of the heated rib, m
L_2 = length of the unheated plate, m
Nu = Nusselt number, $= hD_h/k$
Nu_y = local Nusselt number, based on local height, measured from top of channel A/bottom of channel B to midheight of heated rib
Pr = Prandtl number, $= \nu/\alpha$
Q = power input per heated rib, W
Q_c = convective heat transfer rate, W
Q_L = conduction heat loss, W
Q_r = radiation heat loss, W
Q_{sc} = substrate conduction heat transfer rate, W
Q_t = total power input to each test rib, W
Re = Reynolds number, $= VD_h/\nu$
T = temperature, °C
T_f = reference fluid temperature, $= 0.5\,(T_w + T_o)$, °C
T_o = inlet temperature of air, °C
T_w = local temperature of the heated rib, °C
V = inlet velocity of air, m/s
W = width of the channel, m
x, y, z = Cartesian coordinates, m
α = thermal diffusivity, $= k/\rho C$, m²/s
β = volumetric coefficient of expansion, 1/k
ν = kinematic viscosity, m²/s
ρ = density, kg/m³

Superscript
— = average value

Received Aug. 10, 1989; revision received June 20, 1990; accepted for publication July 3, 1990.

*Graduate Student, Department of Mechanical Engineering.
†Professor and Chairman, Department of Mechanical Engineering. Member AIAA.

Introduction

RECENT technological implications have given rise to increased interest in mixed convection problems in vertical channels. The physical situations involve both buoyancy-assisted and opposed cases for laminar and turbulent flows. Flow systems in a vertical channel are divided into two kinds of systems. Those in which the buoyancy force acts in the same direction as the flow (e.g., a heated upward flow or a cooled downward flow) are termed assisting flows. On the other hand, when the directions are opposite, the systems are called opposing flows. The nature of these two kinds of systems turns out to be intrinsically different, in view of the apparent difference in the distortion pattern of shear stress distributions due to buoyancy near the wall.

A review of the open literature, however, reveals that there has been only scant attention paid to mixed convection in vertical channels. For fully developed laminar flow, theoretical solutions have been obtained by Rao and Morris[1] for both buoyancy-assisted and opposed mixed convection under the condition that one wall is heated at uniform heat flux and the other insulated. For assisted flow, heat transfer was found to increase with the Rayleigh number; for opposed flow, the converse holds true. For hydrodynamically and thermally developing flow, Yao[2] presented an analysis of combined convection with symmetric uniform wall temperature or uniform heat flux condition. His study revealed the flow structure in a developing region and led to the conjecture that reversed flow of a periodic nature could be present in fully developed flow.

For practical applications, during the last decade, the trend in the electronic industry has been toward smaller computer components. This trend has been associated with increasing effects for improving the understanding of heat transfer cooling in electronic components. Typically, the simplest situations have received the primary attention. Natural convection in vertical heated channels has been studied extensively[3-6] to assess the magnitude of the self-induced cooling. Since fans are commonly employed in cooling electronic components, mixed convection in smooth ducts has also been studied.[7-10]

Heat transfer correlations in smooth vertical ducts do not incorporate the effects of the finite disturbance introduced by the presence of the electronic components in the channel. So

far, this effect does not appear to have received much attention in the literature. The objective of this work is to extend the previous studies of mixed convection in a single vectical cavity or channel with discrete heated protrusions on one vertical wall to double vertical channels with two different flow systems. In fact, due to the intervening wall, boundary conditions for these two channels (channels A and B) are different. The intervening wall has a high thermal conductivity in the present study. It will be found that the wall does affect the heat transfer characteristic in channel A and flow pattern in channel B somewhat.

Experimental Apparatus and Procedure

The experimental apparatus consists of double channels with eight alternately unheated and flush-mounted rows of isoflux heated ribs on each channel wall with $H/W = 16$, $D/W = 20$, $L_1/W = 0.51$, $L_2/W = 1.47$, and $W = 50$ mm. The geometry, coordinate system, boundary conditions, and the details of the experimental apparatus are similar to the one in Ref. 11 with a slight change for mixed convection (add a suction blower). The data to be presented are for air ($Pr \sim 0.7$) with approximate power input from $Q = 2.3$ to 71 W per rib. The heated rib wall of the test cell, 800 × 1000 mm, was constructed of 10-mm-thick aluminum sheet ($k = 177$ W/m.K). Sixteen two-dimensional transverse aluminum ($k = 186$ W/m.K) ribs, 25.4 mm wide, 25.4 mm deep, and 1000 mm long, were adhered to the plate. Sixteen slots, 22.2 mm wide, 22.2 mm deep, and 1000 mm long, were cut in these ribs to place 0.4-mm cartridge heaters with an outer diameter of 7.4 mm into a 1.3-mm quartz-made shield. The experiments reported in this paper were conducted using 16 heated ribs with 8 on each channel. Each heater was covered with a 1.6-mm-thick aluminum plate with a heat sink compound (MgO) filled between the heater and the aluminum rib to reduce contact resistance. Thermocouples were then placed in grooves that were milled into each of the heated ribs and unheated sections of the wall. These thermocouples were located at their respective sections, as is also shown in Ref. 11. All of the thermocouples used in the instrumentation were 28-gauge copper-constantan type.

Thermocouples were also placed at different depths in the plexiglass/aluminum plate to estimate the conduction loss. Heater leads and thermocouple wires were passed through the holes made in plexiglass/aluminum plate and were connected to a power panel and a digital data acquisition system, respectively. The power panel consisted of a voltage stabilizer and a step-down transformer. Voltage information for each heated rib was fed to the data acquisition system coupled with a personal computer for data reduction and analysis.

All other sides of the channels were made out of plexiglass, 10 mm thick, and the channel length was $L = 1600$ mm. To form the channel, holes were drilled at four corners of each plate and the plates were bolted together. Channel spacing was maintained and resulted in an aspect ratio of 20 for the cross-sectional area in which the flow was perpendicular. The power in each heater was able to reach ~71 W, i.e., 742.8 W/m^2 for the heated sections.

To examine the flow structure, flow visualization experiments were conducted for several power inputs. A smoke generation method was applied with a $CCl_4 + TiCl_4$ mixture (mixing ratio 1:10) and air as convection medium to visualize the flow. The illumination of the smoke was done by using a slide projector as a light source shining through a narrow slit so as to produce a sheet of light. All photographs were taken with a Canon-T90 camera on Konica SR-V 3200 film with exposure times of 1/8–1/15 s.

In addition to temperature measurements using thermocouples, both channels were placed in the test beam of a laser holographic interferometer for further investigation of the thermal characteristics. The laser holographic interferometry used in this study is essentially the same as that described by Aung and O'Regan[12] and is schematically shown in Ref. 11. Coherent light (0.6328 μm) from a 35-mW Spectra-Physics model 124-B He-Ne laser was split into an object beam and reference beam by a variable silvered mirror, and each beam was expanded to a 90-mm planar wave via a 20x microscopic objective and a 60x microscopic objective and two collimating lenses (diam-12.7 cm). Pinholes of 20-μm diam were located at the focal points of the microscopic objectives in order to eliminate intensity variations in the wave fronts. The two wave fronts intersected at the photographic plate (here at an angle of 30 deg) and produced a hologram when the photographic emulsion was exposed simultaneously to the two beams and then developed in situ. The interferometer components and test section were mounted securely to a 1.4 × 2.0 m vibration-free optical table.

Uncertainty Analysis

A Solartron 3530 Orion automatic data acquisition system was used for data collection. The thermocouple outputs were measured to ±1 μV, which resulted in ±0.01°C sensitivity. A conservative estimate of the accuracy of the temperature measurement is ±0.1°C. The voltage input to each heater circuit was measured with a sensitivity of ±1 mV and an accuracy of ±0.1%. Several runs were conducted where the voltage and current for circuit were measured and the calculated resistance was highly stable. These data indicated a maximum uncertainty of ±1% in the resistance of circuit. The power input to the circuit was then calculated by using the measured voltage drop across the circuit and its respective resistance. This procedure resulted in a maximum uncertainty of ±2% in the calculated power inputs. The uncertainty associated with the length scale used in the data reduction was ±1 mm. The thermophysical properties of the air were assigned an uncertainty of ±3%, which was based on the observed variations in the reported values in the literature.

The overall uncertainty in the Nusselt and Grashof numbers varied with the power input. Smaller power input resulted in a larger uncertainty primarily because of a lower temperature difference across the channel and a higher fraction of energy loss by conduction. As the power input was increased, the uncertainty in the experimental data decreased. The estimated uncertainties in Nu, Re, and Gr were 1.6–5.8, 2.3–5.6, and 1.0–5.4%, respectively. It should be noted that the uncertainty in these parameter was reduced when they were considered in terms of local values since the percent error in the length measurement was decreased.

Data Reduction

The local values of the thermophysical properties of air were obtained at a reference fluid temperature of $T_f = 0.5(T_w + T_o)$. The net convective heat flow rate Q_c, from the test surface to the air in the test channel, was calculated from the following energy balance equation:

$$Q_c = Q_t - Q_L - Q_{SC} - Q_r \quad (1)$$

The conduction losses through various walls of the channels were also calculated to obtain net energy transported by the convective fluid. In general, the conduction loss was within 4.87% of the total input for the present experiments. The substrate conduction heat loss, which was eventually convected to the working fluid in the unheated section, was calculated using a two-dimensional unit cell finite-difference conduction model. The unit cell was chosen from midheight of a heated section to the midheight of the adjacent unheated section. The measured temperatures were used to specify the boundary conditions of the unit cell. The substrate conduction heat transfer was calculated for the heaters where the temperature of the adjacent unheated section was known for all power inputs. For given power inputs, it was found that Q_{SC} was nearly the same (within 1.5%) for these heaters. There-

fore, for each run, all of the heaters were assigned an average value of Q_{SC} based on previous calculations for Q_{SC}. The calculated Q_{SC} varied from 15% (at 2.3 W/heater) to 5% (at 71 W/heater) of the total convected energy. The radiant heat exchanges among all of the side walls Q_r was evaluated using a diffuse gray-surface network.[13] The maximum radiative heat loss was < 4.31% of the total power input for all of the cases investigated.

After Q_L, Q_{SC}, and Q_r were estimated, the net convective heat flow rate Q_c from the rib surface could be obtained. Therefore, the local heat transfer coefficients and Nusselt numbers used in the presentation of the data were calculated by

$$h = Q_c/A_h(T_w - T_o) \qquad (2)$$

where $(T_w - T_o)$ stands for the temperature difference between the rib and the inlet temperature of the air. One may argue whether the temperature difference $(T_w - T_o)$ was still meaningful for the definition of the Grashof number Gr in Gr/Re^2 in channel B. However, for the sake of simplicity and consistency, the same reference temperature $(T_w - T_o)$ was used for both channels A and B even though their flow pattern was quite different after the 180-deg return; we do agree that the effect of the 180-deg return on the flow was quite significant. However, the temperature and velocity measurements just after the 180-deg return in channel B were not easy. These data were not available at this stage. Further study may include this aspect.

Results and Discussion

The present study was conducted for Q = 2.3–71 W/heating element with atmospheric air as the convective medium. The range of Gr/Re^2 varied from 0.12 to 3.51, and the local Prandtl number varied between 0.69 and 0.71. The velocity level for the present study was about 0.18–0.40 m/s.

Flow Visualization

The present results focus on the local steady-state behavior. To assist in explaining the local flow structure, flow visualization was made through a smoke injection method under the steady-state condition. The steady-state condition was determined when the variation of temperature of the rib was < 1% of that of its previous value. It usually took 4–5 h to reach a steady state. In order to obtain a better understanding of the results, a schematic of the major flow structure of the present study is shown in Fig. 1. The channels are identified as channel A (the left channel) and channel B (the right channel). The typical flow patterns visualized in the central portion of both channels are demonstrated in Figs. 2a and 2b for two different Gr/Re^2 values, respectively. At Re = 1321, Figs. 2a and 2b basically show a cell within two consecutive ribs for channels A and B and indicate a buoyancy driven fluid flow within two consecutive ribs. However, the main flow adjacent to the cold wall moved downward/upward, respectively. The cold wall was at a lower temperature for channel A, whereas the temperature of the cold wall for channel B started simultaneously to rise up through a substrate conduction because of the heating element of channel A. In channel B, the main flow moved upward and had the same direction as that of the buoyancy effect. Based on the two different conditions, it was not expected to have the same flow structure in these two channels. Actually, one was opposing the forced flow, and one was assisting the flow.

For a given rib position in channels A and B, the location of the cell separation shear layer was dependent on the ratios of Gr/Re^2. As the Gr/Re^2 increased, the location of the separation layer changed dramatically, as can be seen from Fig. 2b. In fact, in this figure, an unsteady sinuous flow, which at higher Gr resulted in a three-dimensional recirculating pattern adjacent to the heated rib along the channel side wall and in

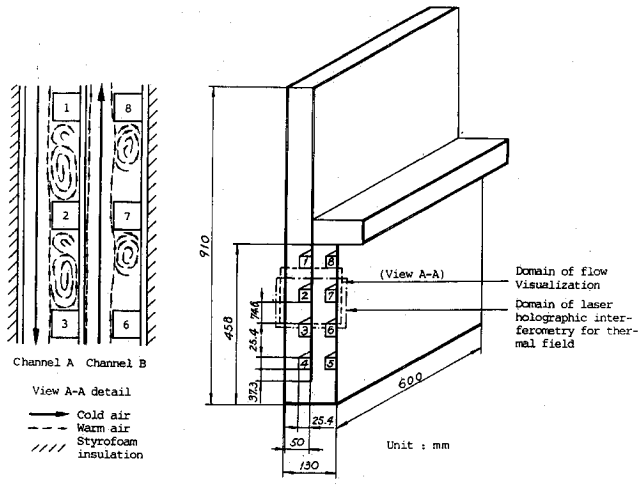

Fig. 1 Domain of flow/thermal fields by optical visualization.

the downward/upward main flow along the center line of the channel was noticed. For Gr/Re^2 = 0.35, a small bubble was observed near the leading edge of the rib in channel A. As Gr/Re^2 increased to 3.51, this small leading-edge bubble disappeared in channel B while the recirculation region behind the rib became smaller. This behavior was expected because, for large Gr/Re^2, the strong buoyant upflow along the vertical surface inhibited the size of the separated bubble. On the other hand, this behavior was not found in channel A. This was because, when the flow was upward (in channel B), separation and reattachment took place on the cold/hot walls and the convective cell extended away from the heated rib. However, in the case of opposing flow, the recirculation occured only on the heated wall. The strength and extent of the convection cell depended on the higher Grashof of number and the larger Reynolds number required for the disappearance of the secondary flow in between the two consecutive heated ribs. The thermal boundary layer became thicker as the Gr/Re^2 increased. The wall plume-like behavior near the channel wall was seen to develop.

The influence of the Reynolds number (at a constant Gr/Re^2) can be seen by comparing the different plots in Figs. 3a and 3b. In view of the stronger motion at Re = 1578, the recirculating bubble is stronger and larger in Fig. 3b as compared to that in Fig. 3a. Furthermore, the thermal boundary layer increases in thickness with decreasing Reynolds number. In general, the present flow patterns are similar to those observed by Habchi and Acharya[14] in their study of laminar mixed convection in a partially blocked, vertical channel with asymmetrically heated ribs. However, no statement can be made with respect to differences in the velocities, or for that matter, the sequence of changes in flow pattern with respect to a common flow parameter.

Qualitative Description of the Temperature Field

Figures 4 and 5 show the interferograms of the temperature field in both channels in the infinite fringe mode for two different cases at Re = 1321 and Gr/Re^2 = 1.20. The resulting fringes are then isotherms. Figure 4 shows the temperature contours near the ribs, whereas Fig. 5 shows the isotherms for the valley between two consecutive ribs.

The measured isotherm patterns in Fig. 4 indicate that the surface heat flux is reduced along the wall just below and just above the heated element as compared with what it would be on a smooth wall. The temperature gradient at the outer surface of the element appears to be high, especially near the upper (for channel A)/lower (for channel B) outside corner. This characteristic is opposite to that reported by Shakerin et al.[15] in their investigation of natural convection in an enclosure with discrete roughness elements on a vertical heated wall.

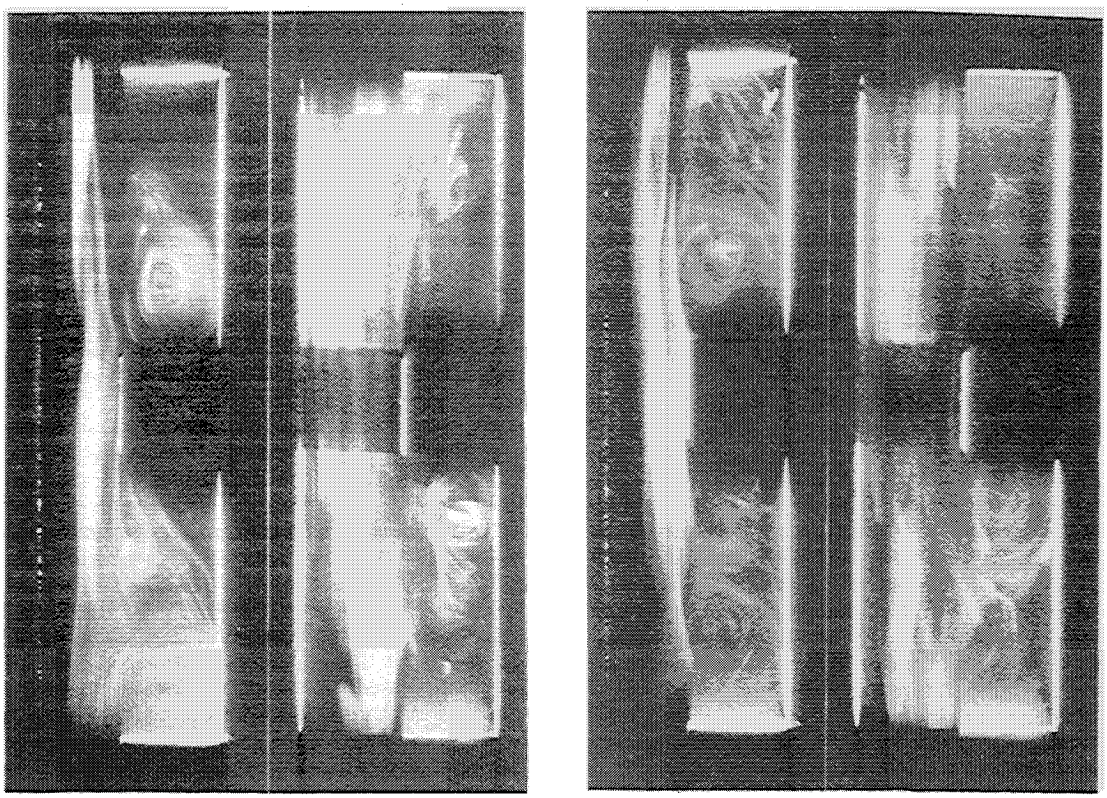

Fig. 2 Photographs made by flow visualization at $Re = 1321$.

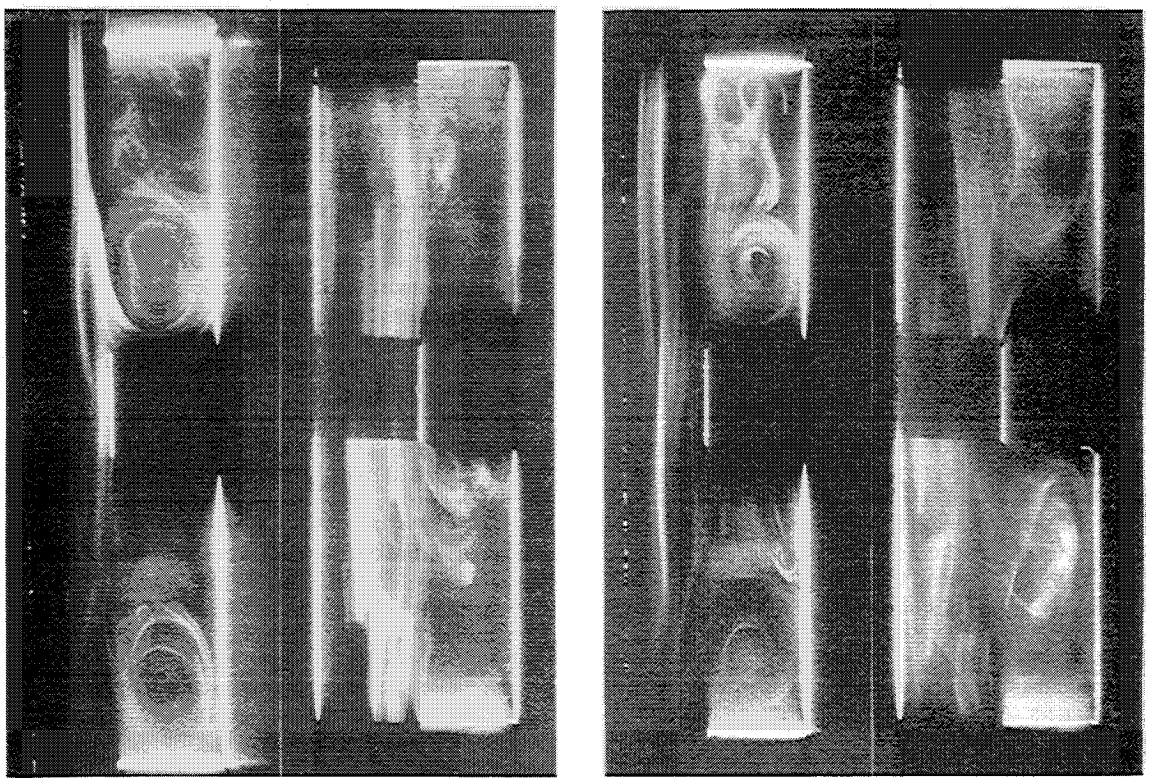

Fig. 3 Photographs made by flow visualization at $Gr/Re^2 = 1.20$.

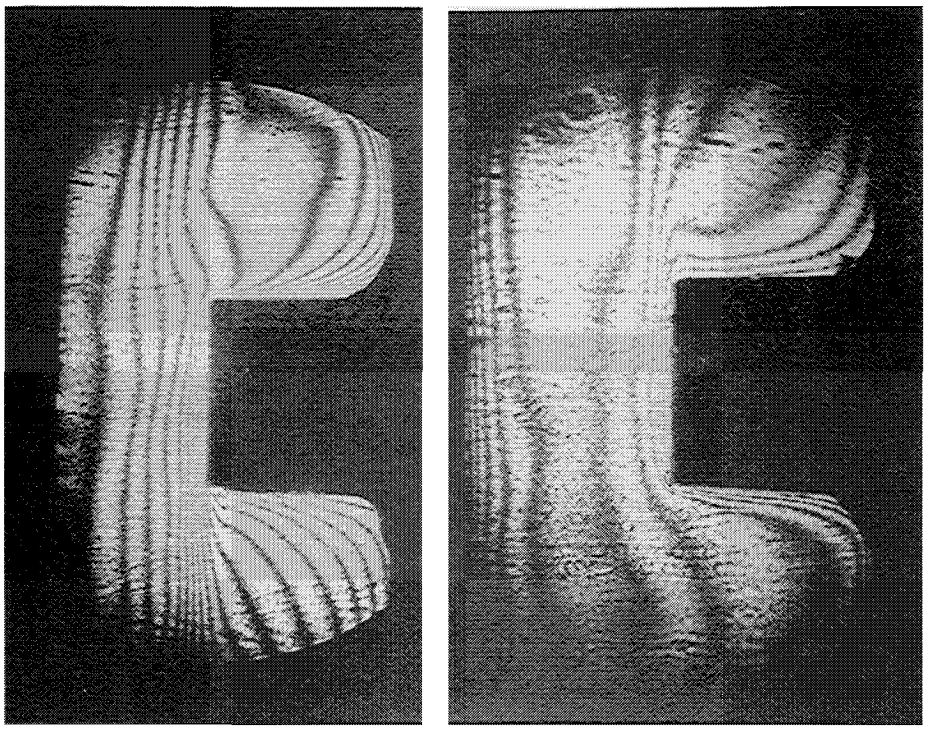

Fig. 4 Interferograms for the flow near the vicinity of the rib at $Re = 1321$.

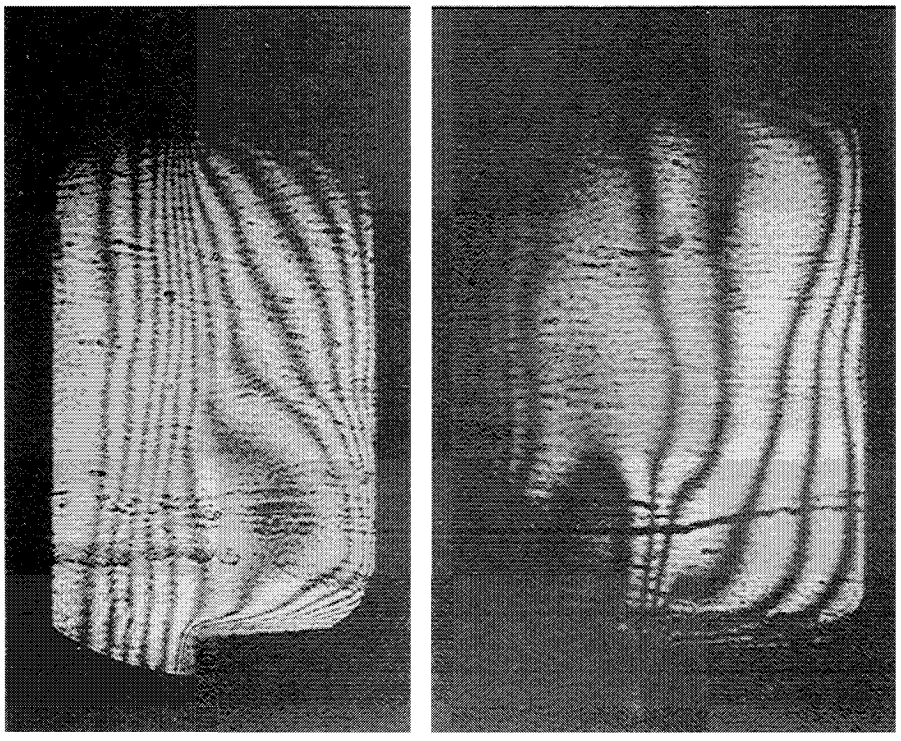

Fig. 5 Interferograms for the flow near the valley of two consecutive ribs at $Re = 1321$.

Furthermore, the present isotherm patterns along the cold wall for both channels agree with the statements for the flow patterns in the preceding section. In Fig. 5, the measured isotherm patterns for both channels in the valley of two consecutive ribs have the same trend at $Re = 1321$ and $Gr/Re^2 = 1.20$, except outside the cavity. This discrepancy is due to the different flow types (one for opposing flow and one for assisting flow). The temperature gradient along the vertical wall of the channel appears to be higher for channel A than that for channel B.

If there is no change in the direction of fluid motion, the width of a fringe will remain constant along its path. When

the fringes become thinner and get closer to each other, a region of high heat transfer exists due to a larger temperature gradient, as can be seen from Fig. 4 for flow along the vertical rib wall in channel B or A. The higher order fringes possess high curvature due to flow separation/recirculation. There is, however, an instability present that can be noticed in Fig. 4 by the thicker arc-shaped phenomenon isotherms for the flow near the upper or lower portion of the ribs. These two characteristics also exist in Fig. 5. Along the vertical walls of the cavity, the fringes are thinner and follow the contour of the cavity. However, away from the wall, due to the recirculation-like flow, arc-shaped isotherms occur elsewhere. Near the center of the recirculation, the fringe is sparsely packed. Incidentally, wall plume-like behavior near the core flow in channel B of Fig. 4 is clearly noted. This also confirms the previous findings based on the flow visualization.

Temperature Distribution

The temperature distributions at different Reynolds numbers, $T_w - T_o$, along the streamwise direction at each rib for both channels for $0.35 \leq Gr/Re^2 \leq 3.51$ are given in Figs. 6 and 7, respectively. Each rib has three thermocouple measurement positions. They are located at front, top floor, and rear face of the rib, respectively.

The temperature of the heated/unheated sections shows a steady increase from heated rib 1 to 16 (i.e., channels A and B). For both channels, nearly constant temperature distribution was found for lower Gr/Re^2 (< 2.37) in Fig. 6. A different thermal behavior of a temperature difference ($T_w - T_o$) followed by a slight rise to a peak value at $0.18 \leq y/H \leq 0.22$, and finally approaching a nearly constant value is observed at $Re = 1321$ in channel A. This phenomenon persists for larger values of Gr/Re^2, for instance, $Gr/Re^2 =$ 3.51. This behavior was noted also in mixed convection in vertical channel for isothermal heated smooth wall with protrusion by Habchi and Acharya[14] and other investigators for forced convection without protrusion. The dependence of the temperature profile on Gr/Re^2 in channel B is similar to that observed in channel A, i.e., temperature increases with increasing Gr/Re^2. This behavior is also observed at $Re = 2675$ (Fig. 7). However, due to the turbulent nature of flow, Fig. 7 shows that the temperature distributions in channels A and B have slight differences from those observed in Fig. 6. The variation of wall (both heated/unheated) temperature depends mainly on changes in the flow pattern (e.g., flow separation/recirculation), flow type (opposing/assisting flow), flow regime (e.g., laminar, transitional, unsteady, and turbulent flows), and slightly on the stratification parameter. Therefore, no single explanation can be drawn at this stage for the measured profiles. The convection heat transfer is dependent on the temperature gradient near the surface, which in turn is strongly influenced by the flow structure (presence of separation/recirculation). Actually, it is expected that, due to the present rib geometry, separation, with flow reversal at wall or at the surface of the rib, was observed in the experiments. In fact, unsteady flow reversal and flow shedding from the rib were noticed for $Gr/Re^2 > 1.10$ at higher Reynolds number. This highly unstable, separated shear layer created in the flow over repeated ribs undergoes rapid transition to turbulence when compared with the wall without ribs, which may augment heat transfer. This will be verified later. Moreover, based on the temperature measurement across the channels,

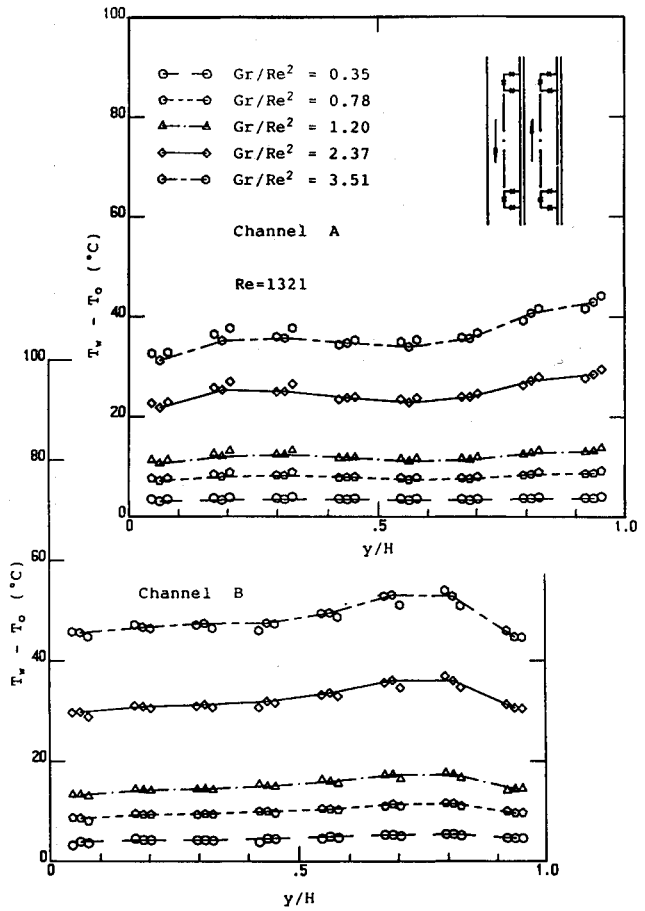

Fig. 6 Streamwise temperature distribution along the rib wall at $Re = 1321$.

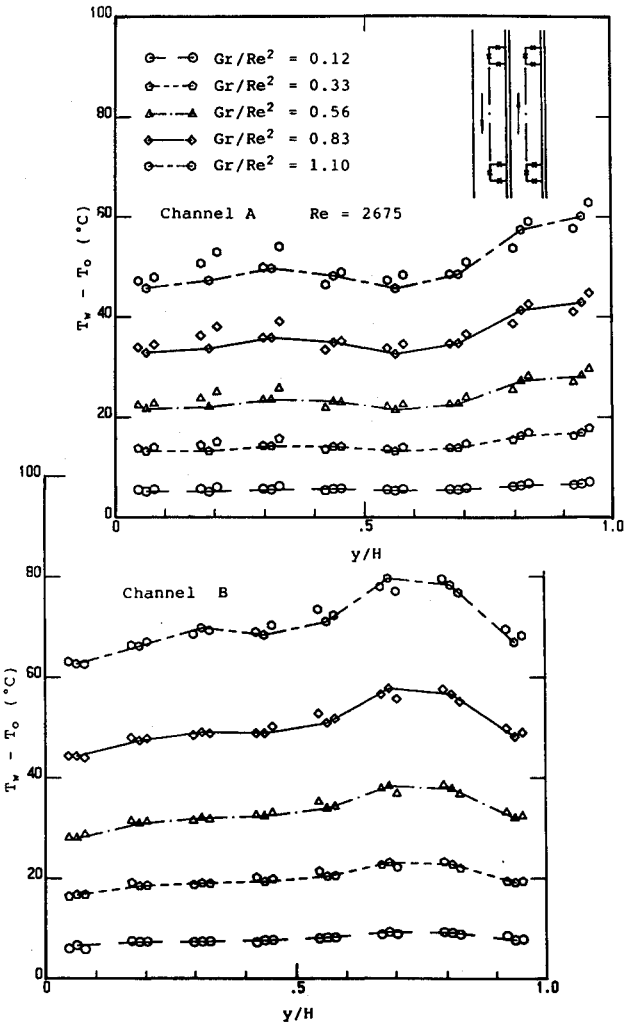

Fig. 7 Streamwise temperature distribution along the rib wall at $Re = 2675$.

it was found that the temperature variation between the positions of ±300 mm from the centerline is < 2% (not shown here).

Local Heat Transfer Rates

Figure 8 presents the local Nusselt number Nu_y plotted against downstream distance for both channels A and B (based on temperature measurement at the front surface of the rib). For a fixed flow rate (or Re = 1321), it is seen that the heat transfer coefficient in channel A generally decreases with increasing distance initially and is followed by a smooth rise to its maximum and, then, decreases thereafter. On the other hand, heat transfer coefficient in channel B initially decreases with increasing distance and finally is followed by a rise to certain value at the outlet of the channel. In general, the Nusselt number attains a maximum value near the inlet of channels A and B and decreases as y/H increases. This is expected because the surface near the entrance is just cooled by the cold fluid. As the fluid flows along the hot surface, its temperature increases and the heat transfer coefficient correspondingly decreases. Along the the vertical surface of the upstream ribs (parallel to the y axis), the same behavior is observed. Beyond the upstream ribs ($y/H \lesssim 0.40$), the Nusselt number behavior is noticeably different in channels A and B due to the size and strength of the recirculating bubble in those regions. The Nusselt number increases up to the point of $y/H \cong 0.42$ and then decreases gradually toward the exit of the channel A. At $y/H \cong 0.42$, the heat flux and, therefore, the Nueselt number values peak. On either side of the point of $y/H \cong 0.42$, the flow is directed outward and the Nusselt number decreases. For assisting flow (in channel B), the recirculation bubble is very small and strong. Therefore, unlike the opposing flow, a monotonic increase toward the exit of channel B is observed.

The influence of Gr/Re^2 in channels A/B should also be noted because the main flow opposes/assists the buoyancy force. For the lower Reynolds numbers (e.g., Re = 1321), as Gr/Re^2 decreases, the strength of the recirculating bubble decreases, leading to lower Nu_y values in channel B. This result is also observed in channel A. Generally, the local Nusselt number distributions at Re = 2675, shown in Fig. 9, have the same trend as that shown in Fig. 10. However, the influence of Gr/Re^2 in channel B has the reverse effect on heat transfer rate as compared to that of Fig. 8. This finding agrees with Churchill's.[16] On the contrary, for channel A, both Re = 1321 and 2675 give higher heat transfer rate as Gr/Re^2 increases. This does not seem to coincide with the statement of Churchill. Furthermore, for both Reynolds numbers, the heat transfer rate in channel A is generally higher than that in channel B. This becomes clearer as Reynolds number becomes higher.

Overall Heat Transfer

Figure 10 shows the data and the four correlations for the average Nusselt number plotted against the Reynolds number for different Gr/Re^2 as the parameter. The correlations are within 7.8% of the original data. These correlation equations are given as,

Channel A:

$$Nu = 0.223Gr^{0.022}Re^{0.648}(D_h/H)^{0.097} \quad (3)$$

Channel B:

$$Nu = 0.145Gr^{0.022}Re^{0.672}(D_h/H)^{0.097} \quad (4)$$

for $1181 \leq Re \leq 1578$ and $0.35 \leq Gr/Re^2 \leq 3.51$, and

Channel A:

$$Nu = 0.113Gr^{0.022}Re^{0.765}(D_h/H)^{0.097} \quad (5)$$

Channel B:

$$Nu = 0.061Gr^{0.022}Re^{0.800}(D_h/H)^{0.097} \quad (6)$$

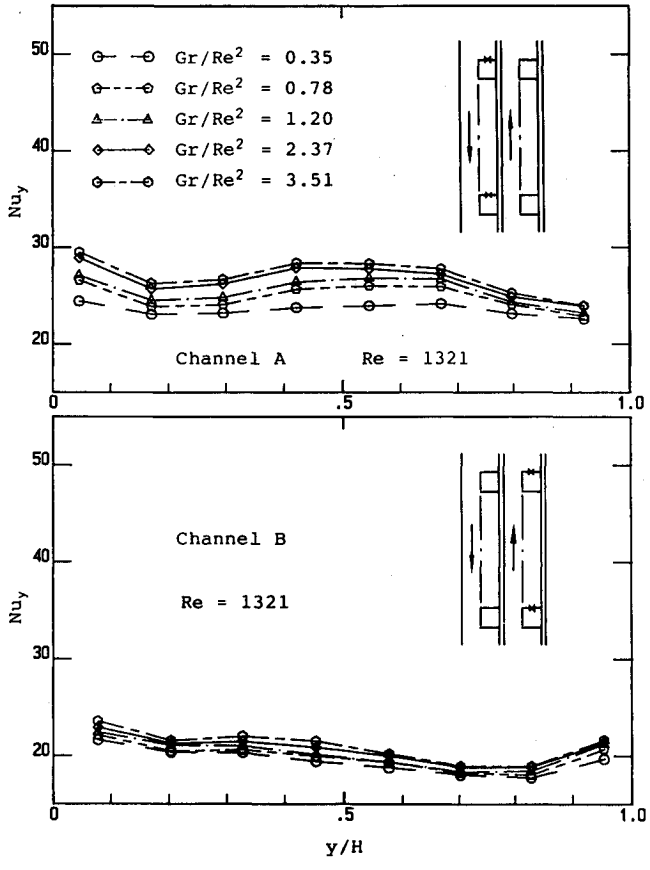

Fig. 8 Local Nusselt number vs downstream distance at Re = 1321.

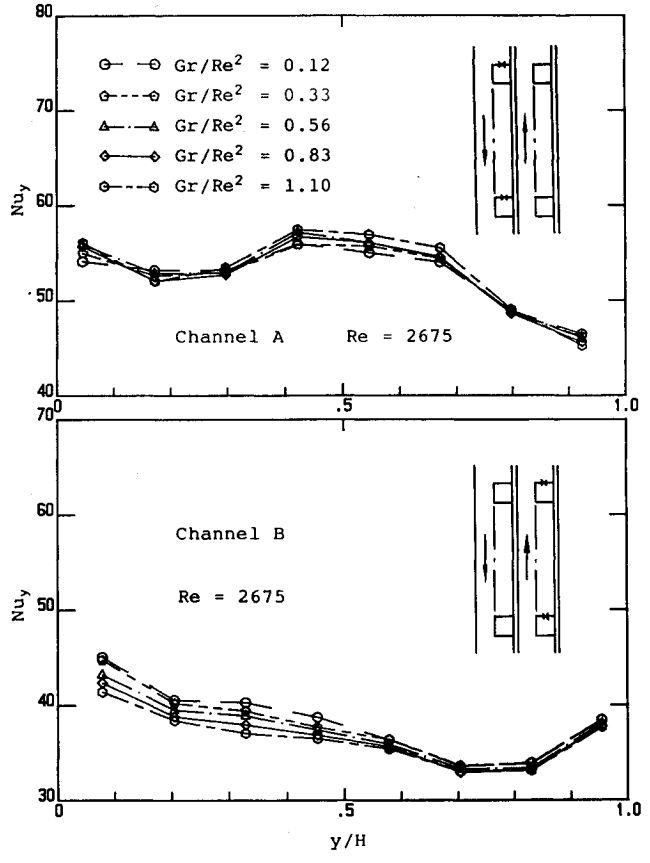

Fig. 9 Local Nusselt number vs downstream distance at Re = 2675.

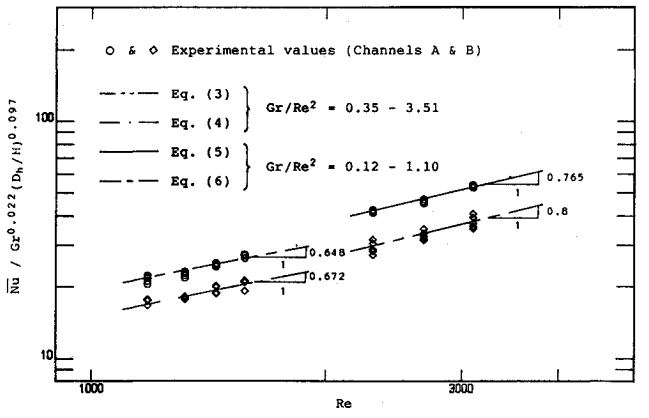

Fig. 10 Plot of average Nusselt number against Reynolds number.

for $2298 \leq Re \leq 3094$ and $0.35 \leq Gr/Re^2 \leq 3.51$.

The slope of the average Nusselt number curve in Fig. 10 depends on Re and increases to 0.8 as the flow regime changes from natural to forced convection (i.e., as Gr/Re^2 decreases). Owing to the lacking of existing data, quantitative comparison was not made with smooth channels (with the same physical geometry).

Conclusions

The nature of mixed convection over discrete asymmetrically heated ribs ($L_1/W = 0.51$, $L_2/W = 1.47$) in a channel with the existence of both opposing/assisting flows, respectively, is investigated in the range $0.12 \leq Gr/Re^2 \leq 3.51$ to broaden our basic understanding of this type of convective heat transfer. The most significant contributions of the present study are the following:

1) Systematic experimental data for steady-state mixed convection heat transfer are obtained and a quantitative heat transfer correlation is established.

2) The flow visualization and the photographs indicate that the existence of a protruding ribs changes the flow characteristics and originates the recirculation zone as well as the turbulence zone in the vicinity of the rib.

3) Generally, the main flow separates from the vertical wall, reattaches afterward, and produces a recirculating, secondary flow in the channel. When the flow is downward, the recirculation occurs in the valley of two consecutive ribs. However, in the case of assisting flow, separation and reattachment take place on the cold wall and the convective cell extends away from the heated rib. The strength and extent of the convective cell strongly depend on the governing parameters.

4) The heat transfer data based on laser holographic interferometry, thermocouple temperature measurements, and flow visualization photographs suggest that flow separation or recirculation is the major factor influencing the temperature of the heated ribs.

5) Based on the analyses of the photographs and interferograms, it is found that, as Gr/Re^2 increases, the recirculation region becomes stronger and smaller for the assisting flow (in channel B), whereas this change is not clear for the opposing flow (in channel A).

6) For higher Reynolds numbers, the local and average Nusselt numbers increase with decreasing Gr/Re^2 in channel B, as confirmed by Habchi and Acharya,[14] whereas in channel A, the opposite trend holds.

7) For channels A and B in both flow regimes (laminar/turbulent), the average heat transfer results were correlated in equation forms that will be useful in the design of electronic cooling devices.

Acknowledgment

The authors would like to thank the National Science Council (NSC) of Taiwan, Republic of China, for financial support under Grant NSC77-0401-E110-07.

References

[1]Rao, T. L. S., and Morris, W. D., "Superimposed Laminar Forced and Free Convection Between Vertical Parallel Plates When One Plate is Uniformly Heated and the Other is Thermally Insulated," *Proceedings of Institution of Mechanical Engineers*, Vol. 182, Pt. 3H, 1967–68, pp. 374–381.

[2]Yao, L. S., "Free and Forced Convection in the Entry Region of a Heated Vertical Channel," *International Journal of Heat and Mass Transfer*, Vol. 26, No. 1, 1983, pp. 65–72.

[3]Aung, W., "Fully Developed Laminar Free Convection Between Vertical Parallel Plates Heated Asymmetrically," *International Journal of Heat and Mass Transfer*, Vol. 15, No. 8, 1972, pp. 1577–1580.

[4]Nakamura, H., Asoko, Y., and Naitou, T., "Heat Transfer by Free Convection Between Two Parallel Flat Plates," *Numerical Heat Transfer*, Vol. 5, No. 1, 1982, pp. 39–58.

[5]Aung, W., Fletcher, L. S., and Sernas, V., "Developing Laminar Free Convection Between Two Parallel Flat Plates with Asymmetric Heating," *International Journal of Heat and Mass Transfer*, Vol. 15, No. 10, 1972, pp. 2293–2308.

[6]Kettlehorough, C. F., "Transient Laminar Free Convection Between Heated Vertical Plates Including Entrance Effects," *International Journal of Heat and Mass Transfer*, Vol. 15, 1972, pp. 883–896.

[7]Cebeci, T., Khattab, A. A., and Lemont, R., "Combined Natural and Forced Convection in Vertical Ducts," *Proceedings of the Seventh International Heat Transfer Conference*, Munich, FRG, Vol. 2, 1982, pp. 419–424.

[8]Dalbert, A. M., "Natural, Mixed and Forced Convection in an Vertical Channel with Asymmetric Uniform Heating, Proceedings of the Seventh International Heat Transfer Conference, Munich, FRG, Vol. 1, 1982, pp. 97–105.

[9]Quintiere, J., and Huller, W. K., "An Analysis of Laminar Free and Forced Convection between Parallel Plates," *Journal of Heat Transfer*, Vol. 95, No. 1, 1973, pp. 53–59.

[10]Chen, T. S., Armaly, B. F., and Ali, M. M., "Turbulent Mixed Convection Along a Vertical Plate," *Journal of Heat Transfer*, Vol. 109, No. 2, 1987, pp. 251–253.

[11]Lin, T. Y., and S. S., Hsieh, "Natural Convection of Opposing/Assisting Flow in Vertical Channels with Asymmetrically Discrete Ribs," *International Journal of Heat and Mass Transfer*, Vol. 33, No. 10, 1990, pp. 2295–2310.

[12]Aung, W., and O'Regan, R., "Precise Measurement of Heat Transfer Using Holographic Interferometry," *Review of Scientic Instruments*, Vol. 42, 1971, pp. 1755–1758.

[13]Siegel, R., and Howell, J. R., *Thermal Radiation Heat Transfer*, 2nd edition, McGraw-Hill, New York, 1981.

[14]Habchi, S., and S. Acharya, "Laminar Mixed Convection in a Partially Blocked, Vertical Channel," *International Journal of Heat and Mass Transfer*, Vol. 29, No. 11, 1986, pp. 1711–1722.

[15]Shakerin, S., Bohn, M., and Loehrke, R. I., "Natural Convection in an Enclosure with Discrete Roughness Elements on a Vertical Heated Wall," *International Journal of Heat and Mass Transfer*, Vol. 31, No. 7, 1988, pp. 1423–1430.

[16]Churchill, S. W., "Combined Free and Forced Convection in Channels," *Heat Exchanger Design Handbook*, Vol. 2, Hemisphere, Washington, DC, 1983, pp. 1–12.